THE ASTROPHYSICAL JOURNAL, 462:13–24, 1996 May 1

EVOLUTION OF CLUSTERS IN COLD PLUS HOT DARK MATTER MODELS

CHARLES WALTER AND ANATOLY KLYPIN
Department of Astronomy, New Mexico State University, Las Cruces, NM 88003-0001
Received 1994 June 23; accepted 1995 October 20

ABSTRACT

We use N-body simulations to study the evolution of galaxy clusters over the redshift interval $0 \leq z \leq 0.5$ in cosmological models with a mixture of cold and hot dark matter. Five different techniques are utilized: the cluster-cluster correlation function, axial ratios and quadrupoles of the dark matter distribution in individual clusters, virial properties, and density profiles. We find that the correlation function for clusters of the same mass limit was larger and steeper at high redshifts. The slope increases from 1.8 at $z = 0$ to 2.1 at $z = 0.5$. The comoving correlation length r_c scales with the mass limit M within a comoving radius 1.5 h^{-1} Mpc and the redshift z as $r_c \approx 20(1 + z)(M/M_*)^{1/3}$, where $M_* = 3 \times 10^{14}\ h^{-1}\ M_\odot$. When the correlation length is normalized to the mean cluster separation d_c, it remains almost constant: $r_c \approx (0.45\text{–}0.5)d_c$. For clusters of small masses ($M < 2 \times 10^{14}\ h^{-1}\ M_\odot$), there is an indication that r_c goes slightly above this relation, with the constant of proportionality being $\sim$0.55–0.6.

Anisotropy of density distribution in a cluster shows no change with redshift, with axial ratios remaining constant at $\sim$1.2. In other words, clusters at present are as elongated as they were at $z = 0.5$. While the anisotropy of clusters does not change with time, the density profile shows visible evolution: the slope of the density profile changes from $\gamma \approx -3.5$ at $z = 0.5$ to $\gamma \approx -2.5$ at the present. We find that the core of a cluster remains essentially the same over time but the density of the outlying regions increases noticeably. The virial relation $M \sim v^2$ is a good approximation, but there is a large fraction of clusters with velocity dispersions greater than given by this relation, and clusters with the same rms velocities have smaller masses in the past, by a factor of 2 at $z = 0.5$.

Subject headings: cosmology: theory — dark matter — galaxies: clusters: general — large-scale structure of universe — methods: numerical

1. INTRODUCTION

The distribution of galaxy clusters can provide a great deal of insight as to the structure of the universe. By comparison with real data such as the Abell (1958), Automatic Plate Measuring (APM; Dalton et al. 1992), or Edinburgh-Durham (Nichol et al. 1992) cluster catalogs, the validity of many cosmological models can be determined. While in the past we were mainly interested in properties of clusters at $z = 0$, new observational results will bring more information regarding the evolution of cluster properties. Among interesting tests, there are "traditional" tests such as evolution of the correlation function and the mass function. It is also interesting to look for more detailed information. Statistics such as elongation of clusters and density profiles could shed light on the rate of evolution of fluctuations and thus the mean density of the universe and the nature of dark matter.

Many different cosmological models have been proposed to address these issues. Among these are the standard cold dark matter (CDM) model, CDM with a cosmological constant $\Omega_\Lambda = 0.5\text{–}0.8$, and the cold and hot dark matter (CHDM) model, with 20%–30% of mass in the form of hot dark matter (presumably massive neutrinos). The CHDM model (see Klypin et al. 1993 for references) was shown to fit reasonably well the available data on cluster properties at $z = 0$. For example, Holtzman & Primack (1993), using the peaks formalism for Gaussian density fields, found that the correlation function of clusters in the CHDM model is consistent with the correlation function of Abell clusters. Later, their results were confirmed by N-body simulations for Abell clusters (Jing et al. 1993; Klypin & Rhee 1994, hereafter KR94; but see also Cen & Ostriker 1994) and for APM clusters (KR94; Dalton et al. 1994). Borgani, Coles, & Moscardini (1994) and Borgani et al. (1995) came to the same conclusion, using the Zel'dovich approximation. The CHDM model predicts (see, e.g., KR94; Borgani et al. 1994) a cluster mass function that is in agreement with the results of White et al. (1993b) and Biviano et al. (1993) for Abell clusters.

There are other techniques available to examine clusters with different masses. Bartlett & Silk (1993), KR94, and Jing & Fang (1994) estimated the distribution function of gas temperature in galaxy clusters by using either the Press-Schechter approximation or N-body results in conjunction with the temperature–velocity dispersion relation. The temperature distribution function was estimated by Bryan et al. (1994) based on N-body plus hydrodynamic simulations. The velocity dispersion function is another way to measure the abundance of different clusters (Jing & Fang 1994). All the tests favor the CHDM model. The real problem for the model is related to the amount of gas in clusters. Estimates based on X-ray observations indicate that the ratio of baryonic mass to total cluster mass is in the range $M_b/M_{\rm tot} = 0.1\text{–}0.25$ for the assumed Hubble constant $H_0 = 50$ km s^{-1} Mpc^{-1} (White et al. 1993b; White & Fabian 1995). This is significantly larger than the upper limit $\Omega_b < 0.1$ predicted from primordial-nucleosynthesis calculations (Walker et al. 1991; Krauss & Kernan 1994). CHDM models with two or three neutrinos can slightly ease this problem compared to models with just one massive neutrino because the massive neutrinos are too hot and avoid the central $\sim$1 Mpc region of galaxy clusters. This results in a decrease in the amount of dark matter in the central parts of clusters by at most 20%–30%, increasing the expected ratio of baryons to dark matter to 0.12–0.13.

The CHDM model with 30% of mass in neutrinos has severe problems in explaining the amount of neutral gas in high-redshift ($z > 3$), damped Lyα clouds (Klypin et al. 1995, and references therein). More promising versions of the CHDM scenario with less mass in the hot component (Ma & Bertschinger 1994; KR94; Primack et al. 1995) predict significantly more high-redshift objects, thus making the model compatible with observational data. At the same time, the new variants of CHDM keep the shape of the spectrum and the amplitude of fluctuations on cluster scales of 10–100 Mpc almost the same as in the old CHDM model, which makes the analysis of clusters in the old CHDM model still interesting.

The correlation function of galaxy clusters is still an interesting and controversial test. Recent estimations of the correlation length for Abell clusters give $r_c \approx 20$–$22\ h^{-1}$ Mpc (e.g., Peacock & West 1992; Postman, Huchra, & Geller 1992), which is slightly less than the old estimate, $r_c \approx 25\ h^{-1}$ Mpc, of Bahcall & Soneira (1983) and Klypin & Kopylov (1983). Results of the APM survey show systematically lower values, $r_c \approx 13$–$14\ h^{-1}$ Mpc (Dalton et al. 1992, 1994). This difference has been attributed to inhomogeneities in the selection of Abell clusters (e.g., Sutherland 1988) and to differences in the richness or number density of Abell and APM clusters (Bahcall & West 1992). The dependence of r_c on mass and number of clusters is not well defined in either observational data or theoretical models. Bahcall & Burgett (1986), Bahcall & Cen (1992), and Bahcall & West (1992) argued that $r_c = 0.4 d_c$, where d_c is estimated as $n_c^{-1/3}$, n_c being the number density of clusters. The situation with observational results is unclear. If we take APM results (Dalton et al. 1992, 1994), Edinburgh-Durham results (Nichol et al. 1992), *and* estimates for Abell clusters (Bahcall & West 1992), then all the data seem to be consistent with the relation $r_c = 0.4 d_c$. *Without* the Abell clusters, though, the APM and Edinburgh-Durham results do not indicate the scaling and are consistent with no dependence on the mean separation. Unfortunately, the range of d_c is quite small in this case, so it is difficult to say if there is a contradiction between these two results. From the theoretical side, the problem is no easier. Results from different simulations are somewhat contradictory. A dependence of r_c on d_c or mass of clusters has been found for different cosmological models (e.g., Borgani et al. 1994; KR94; Croft & Efstathiou 1994), but none of the discussed cosmological models show a perfect $r_c \propto d_c$ relation (Croft & Efstathiou 1994; Borgani et al. 1994).

Although many problems of the physics involved in clusters in the present are still unresolved, it is still very possible to examine the observational differences expected in high-z clusters (see, e.g., Gunn 1990; Luppino & Gioia 1995; Thimm & Belloni 1994; Castander et al. 1994). There are indications that some of the high-z clusters could be just projection effects (Thimm & Belloni 1994). Some of them are real, but not very bright (Nichol et al. 1994; Castander et al. 1994). At the same time, it seems that there exist X-ray–luminous clusters already at $z \approx 0.5$, which can pose significant problems for cosmological models.

This paper is organized as follows: In § 2 the methods of simulating the clusters and the criteria for cluster selection are described. The evolution of the correlation function over redshift is covered in § 3. Section 4 details two different methods for measuring shapes of clusters, and § 5 evaluates the evolution of virial properties.

2. SIMULATIONS AND CLUSTER-FINDING ALGORITHM

Most of the results presented in this paper are based on three N-body simulations. All three were of the CHDM model with $\Omega_{\rm CDM} = 0.6$, $\Omega_\nu = 0.3$, and $h = 0.5$. All simulations are scaled to the Hubble constant $H_0 = 100\ h$ km s^{-1} Mpc^{-1}. The first two were of box length $200\ h^{-1}$ Mpc and are described by KR94. The third simulation was of a box of length $255\ h^{-1}$ Mpc, with a 768^3 mesh, 256^3 cold particles, and 2×256^3 hot particles. This yields a spatial resolution of $0.33\ h^{-1}$ Mpc, with each particle having a mass of $5.43 \times 10^{11}\ h\ M_\odot$. The amplitude of angular fluctuations of the microwave background is chosen in such a way that the quadrupole is normalized to 17 μK, which is consistent with *COBE* measurements for the Harrison-Zel'dovich spectrum. This gives an amplitude of mass fluctuations on an $8\ h^{-1}$ Mpc scale of $\sigma_8 = 0.665$. Simulations were run from $z_0 = 13.2$ to the present, with position, mass, and velocity data saved at three epochs, $z = 0$, 0.16, and 0.52. The $200\ h^{-1}$ Mpc boxes have data at $z = 0$, 0.20, and 0.30.

In addition, we use the results of one small-box, high-resolution simulation to address the question of the evolution of cluster internal structure. In this case the simulation was performed for a $50\ h^{-1}$ Mpc box with an 800^3 mesh (the resolution is $62.5\ h^{-1}$ kpc), using 256^3 cold particles and 2×256^3 hot particles. The CHDM model with two equal-mass neutrinos accounting for $\Omega_{\rm hot} = 0.20$, baryon density $\Omega_b = 0.075$, $h = 0.5$, and a cosmic microwave background radiation quadrupole of 18 μK was used.

Clusters were determined as the maxima of mass within a comoving radius of $1.5\ h^{-1}$ Mpc. The choice of the algorithm was motivated by the definition of Abell clusters. We did not try to mimic the observational procedure, specifically, projection effects. This certainly can produce some differences by boosting the "observed" mass of clusters. In this paper we neglect effects of projection, which we will address in a separate paper. In addition, our technique avoids the problems associated with the limiting magnitude involved with observations. Figure 1 presents an example of cluster identification. It shows two two-dimensional projections of CDM particles and identified clusters in a $22.5\ h^{-1}$ Mpc cube from the $255\ h^{-1}$ Mpc simulation at $z = 0$. The distribution in the left panel (x-y projection) indicates that there is a quite large supercluster, which extends almost diagonally from the top left corner to the bottom right corner. The crowded distribution of clusters around $x = 220$–230 Mpc nicely illustrates the difficulty of identification of clusters in projection when the supercluster is seen edge-on. In the right panel (y-z projection), the supercluster is almost face-on. It is clear that the clump of clusters is really a large filament. The figure also shows that clusters have a strong tendency to be found in the most dense regions of the supercluster. For example, the filament at $z = 400$–420 Mpc, $y = 395$ Mpc does not have any identified clusters with mass above $2.5 \times 10^{14}\ h^{-1}\ M_\odot$, while its heavier analog at $y = 365$ Mpc has six clusters. About half the clusters found in Figure 1 have visible substructure. The most massive cluster, at the top of both panels, looks like a double cluster (*right*). Its mass is $2.5 \times 10^{15}\ h^{-1}\ M_\odot$, and its axial ratio is $a/c = 1.4$ (see § 4). There is no obvious tendency for large clusters to have more substructure as compared with small ones. For example, the second-largest cluster on the plot, with mass $1.6 \times 10^{15}\ h^{-1}\ M_\odot$, does look

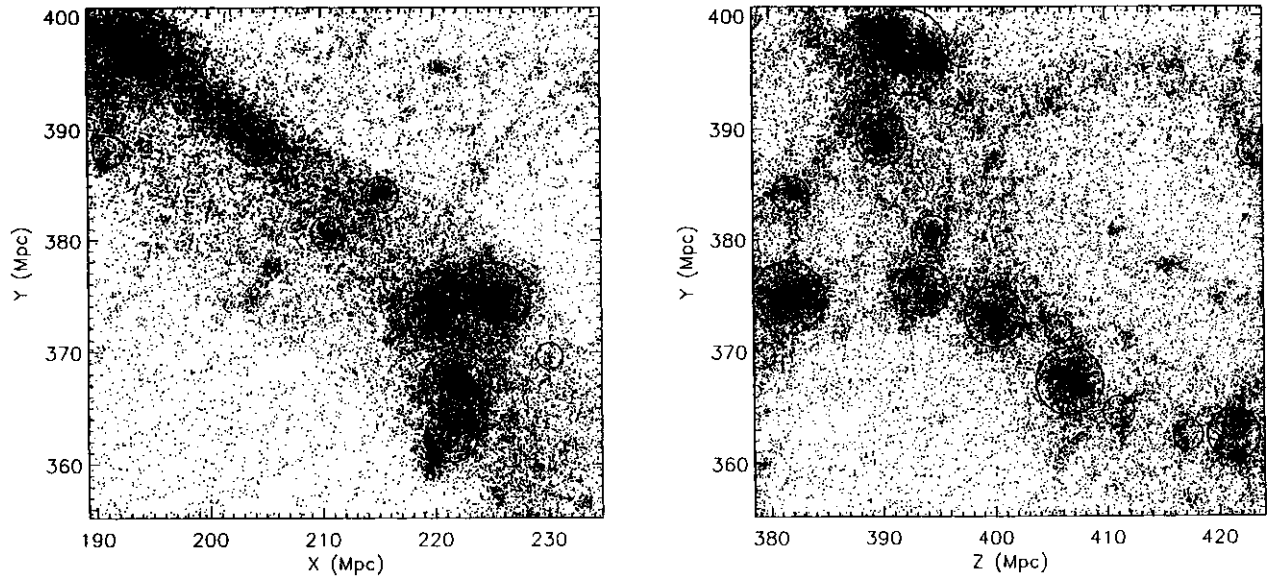

FIG. 1.—Two two-dimensional projections of a box with length 22.5 h^{-1} Mpc from the 255 h^{-1} Mpc sample, showing CDM particles. Distances on the plot are scaled to $h = 0.5$. Five clusters used as examples are taken from this here, ranging in mass from 2.2×10^{14}–$1.6 \times 10^{15}\ M_{\odot}$. Clusters are denoted by circles surrounding the core. The area of each circle is proportional to the mass of the cluster.

quite round (axial ratio 1.1–1.2). Many small clusters show significant deviation from sphericity.

The number of clusters is an important characteristic, which can be used to discriminate different models. In Figure 2 we present the mass function of clusters in our simulations (*solid curve*) and predictions of the Press-Schechter approximation (*dot-dashed curve*). The determination of the masses of galaxy clusters is still uncertain, even for the best-studied cases. An example of this is the estimates of the mass of the Coma Cluster. From analysis of X-ray and optical data, Hughes (1989) gives a mass within the Abell radius of $0.65 \times 10^{15}\ h^{-1}\ M_{\odot}$ with uncertainty of $\sim 30\%$. White et al. (1993b) arrived at the larger value $1.1 \times 10^{15}\ h^{-1}\ M_{\odot}$.

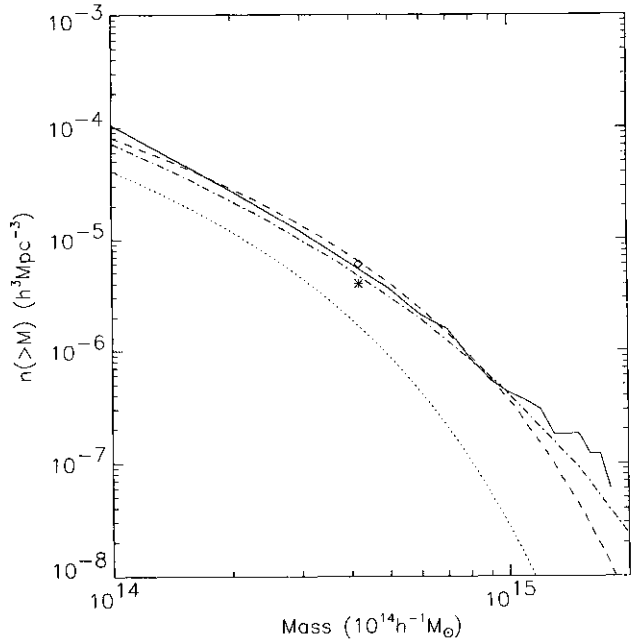

FIG. 2.—Comparison of mass functions. The cluster mass function of our 255 h^{-1} Mpc box is shown by the solid curve. Abell clusters estimated by Bahcall & Cen (1992) are displayed two ways. The dotted curve represents their estimation, while the dashed curve represent the mass scale increased by a factor of 1.6. The dot-dashed curve is the mass function predicted by the Press-Schechter approximation with parameter $\delta_c = 1.5$ and Gaussian filter. The diamond and asterisk at $M = 4.2 \times 10^{14}\ h^{-1}\ M_{\odot}$ represent results by Biviano et al. (1993) and White et al. (1993).

Bahcall & Cen (1993) estimated the mass function of clusters using two methods: (1) galaxy counts, assuming a constant mass-to-light ratio $M/L = 300\ h$ for all clusters, and (2) conversion of the temperature distribution function into the mass function by assuming a simple relation $M \propto v \propto T$. Their results are shown as the dotted curve. More accurate estimates of the mass function were obtained by White et al. (1993a) and Biviano et al. (1993). Unfortunately, those results give the mass function only for one point: the number of clusters more massive than $M_{cl} \equiv 4.2 \times 10^{14}\ h^{-1}\ M_{\odot}$. White et al. (1993a) estimated a cluster abundance of about $n_{cl} = 4 \times 10^{-6} (h^3\ \mathrm{Mpc}^{-3})$. Biviano et al. (1993) gave a slightly higher estimate for the same mass limit: $n_{cl} = 6 \times 10^{-6} (h^3\ \mathrm{Mpc}^{-3})$. Both results are higher than the value found by Bahcall & Cen. It might be possible that Bahcall & Cen systematically underestimated the cluster masses. The dashed curve in Figure 2 shows their results with the mass scale increased by a factor of 1.6—it nicely matches the predictions of the cosmological model and is consistent with the results of White et al. (1993a) and Biviano et al. (1993).

If we assume that Abell richness class 0 corresponds to a mass limit of $M > 2.5 \times 10^{14}\ h^{-1}\ M_{\odot}$, then in the 255 h^{-1} Mpc model we find 297, 121, and 13 "Abell" clusters at the three redshifts 0, 0.16, and 0.52, respectively. For a discussion of cluster masses in different models, see Borgani et al. (1995).

3. EVOLUTION OF CORRELATION FUNCTION OF CLUSTERS

The correlation function can be useful to describe clustering on different scales. We examine the correlation function over time. At the higher redshifts there are very few clusters that meet our fiducial estimate $M > 2.5 \times 10^{14}\ h^{-1}\ M_{\odot}$ for the mass of a richness 0 cluster. In order to obtain enough clusters to have meaningful statistics for this

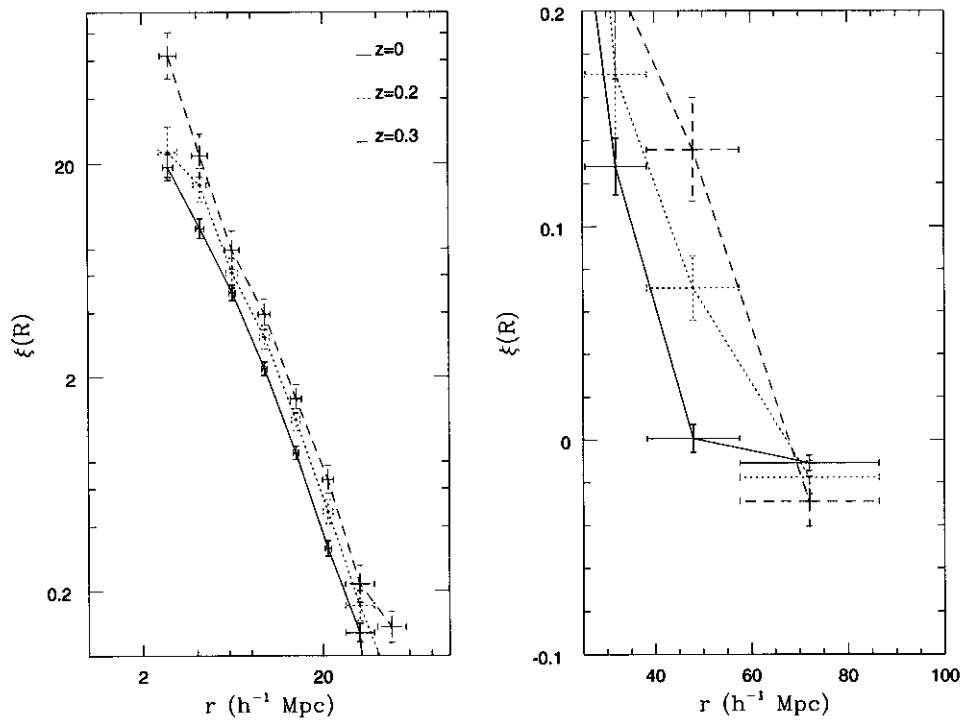

FIG. 3.—Two-point cluster-cluster correlation function ξ in log (*left*) and linear (*right*) scales for two simulations using 200 h^{-1} Mpc periodic boxes at three different redshifts. Vertical errors are calculated from $\sigma = (1 + \xi)/N_p^{1/2}$, where N_p is the number of pairs counted in a given annulus. Horizontal errors for radii less than 25 h^{-1} Mpc come from ξ and a power-law slope computed between 2.5 and 25 h^{-1} Mpc. Beyond 25 h^{-1} Mpc, horizontal errors show the bin size, which is defined as $\Delta r/r = 0.4$.

analysis, we used half the mass limit. Evolution for the 200 h^{-1} Mpc box is shown in Figure 3. Figure 4 is for the bigger box, and it shows the same trend of increasing correlation function at greater redshifts. This implies that clustering *increased* in the past while the number of clusters dramatically decreased. This result can be understood better when the mean separation of clusters in comoving coordinates is considered. Since the number density of clusters decreases with increasing redshift, it is instructive to compare the mean separation d_c with the correlation length r_c, defined by computing a power law over the region 2.5–25 h^{-1} Mpc: $\xi = (r/r_c)^{-\alpha}$. The Levenburg-Marquardt method for finding

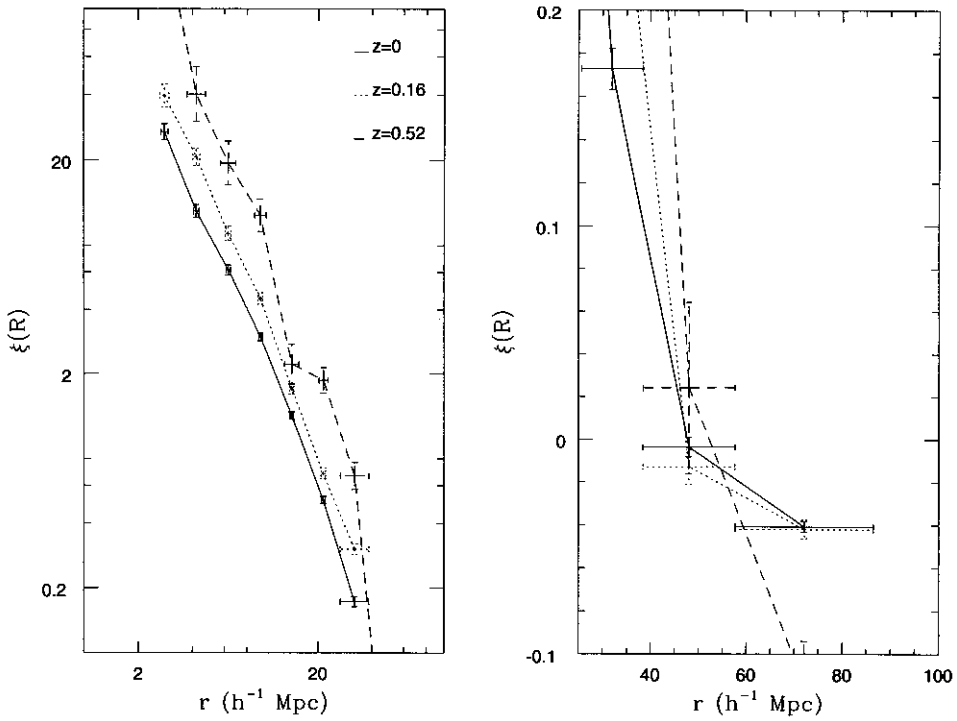

FIG. 4.—Same as Fig. 3, but for a different simulation involving a 255 h^{-1} Mpc box with 3 times the resolution of the first sample. As in Fig. 3, there is a large ξ at greater redshift. The $z = 0.52$ curve suffers from poor statistics, but still follows the general trend.

the minimum in χ^2-space is used to solve simultaneously for the correlation length r_c and the slope α (Press et al. 1992). In Figure 5, correlation lengths are plotted as a function of mass limit. This displays the effects that different mean separations have on clustering. For all redshifts, the correlation length increases, showing increasing amplitude of the correlation function for smaller number densities (and larger masses), which can be seen in Figures 3 and 4 at high redshifts. One effect that may be significant is the increase in steepness of the slope of the $r_c(M)$ relation with redshift. Figure 6 shows the ratio r_c/d_c as a function of mass limit. This value does not equal 0.4 but remains constant near 0.46 ± 0.03 for the $z = 0$ case for mean separations ranging from 33.1 h^{-1} Mpc at a mass limit of $2 \times 10^{14}\ h^{-1}\ M_\odot$ to 49.2 h^{-1} Mpc at a limit of $3.5 \times 10^{14}\ h^{-1}\ M_\odot$. The comoving correlation length r_c scales with the mass limit M within the comoving Abell radius 1.5 h^{-1} Mpc and the redshift z approximately as $r_c \approx 20(1 + z)(M/M_*)^{1/3}$, where $M_* = 3 \times 10^{14}\ h^{-1}\ M_\odot$.

4. SHAPES OF CLUSTERS

We study the evolution of cluster shapes using the 255 h^{-1} Mpc simulation at redshifts $z = 0$, 0.16, and 0.52 by two separate techniques. First, the moment of inertia for each cluster is computed by summing contributions for all cold particles within the radius limit and solving for principal axes. The ratio of the major to minor axis of the inertia tensor is used to characterize the shapes of clusters. Second, we examine the overall quadrupoles Q_2 of the clusters. We define the multipole Q_l as follows (Peebles 1980, § 46):

$$Q_l^2 = \sum_{m=-l}^{l} [a_l(m)]^2\ , \quad a_l(m) = \frac{\sum_{j=1}^{N} Y_l^m(\theta_j, \varphi_j)}{N}\ , \qquad (1)$$

where Y_l^m are spherical harmonics and the summation is over all dark particles N within the radius limit and over all components m of the multipole. The normalization of the multipoles Q_l is defined in such a way that the maximum value of a multipole is 1, which happens when all particles are colinear. Typical values for a quadrupole $Q = Q_2$ are 0.1–0.2. Both statistics are very simple to implement. They test basically the same property, but in a slightly different way.

In Figure 7, we have split each cluster into two sections, the inner core ($r < 0.75\ h^{-1}$ Mpc) and the outer annulus ($0.75\ h^{-1}$ Mpc $< r < 1.5\ h^{-1}$ Mpc). Poor statistics (only 13 clusters) mar the $z = 0.52$ data, but it is clear that in all cases the outer annulus is slightly more anisotropic, suggesting perhaps that relaxation has not been completed. One might expect that newborn clusters at high z would be less relaxed and thus more elongated. Our results indicate that there is no evidence for a general trend with redshift: clusters are as elongated at high z as at the present. For both epochs $z = 0$ and $z = 0.16$, with ample statistics, the inner core peaks at an axial ratio of 1.2 and the outer annulus at 1.3. One effect that may show some relaxation over time is the fact that the percentage of clusters with axial ratio greater than 1.4 decreases. At $z = 0.16$ the inner and outer parts have 17.4% and 37.2%, respectively, whereas at $z = 0$ this drops to 11.7% and 22.6%. Figure 8 shows the quadrupole for the same clusters, again with no definite trend. Peaks for the three samples occur at 0.10, 0.13, and 0.17, in increasing redshift. The distribution of quadrupoles is well approximated by the following expression:

$$\frac{dN}{dQV}(Q) = \frac{N}{V}\left(\frac{2}{\pi}\right)^{1/2}\frac{Q^2}{\sigma^3}\exp\left(-\frac{Q^2}{2\sigma^2}\right), \qquad (2)$$

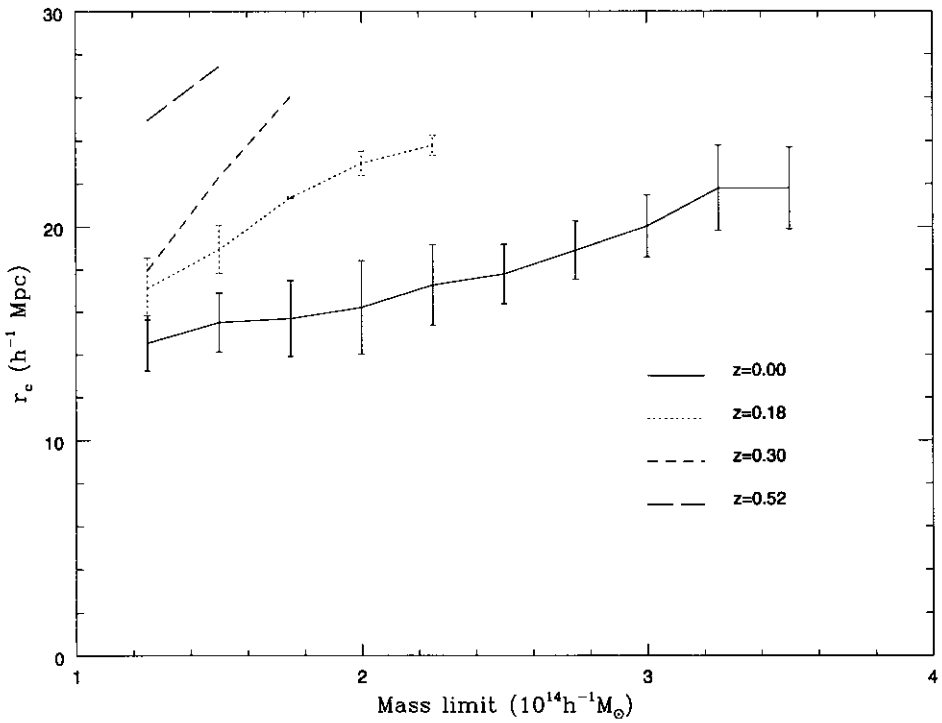

FIG. 5.—Correlation length vs. the mass limit for cluster definition. The correlation length is defined using the power-law fit in the region (2.5–25 h^{-1} Mpc). The lines for $z = 0$ and $z = 0.18$ represent averages of data from two 200 h^{-1} and one 255 h^{-1} Mpc simulations. The error bars extend from one data point to the other. Typically twice as many clusters in the 255 h^{-1} Mpc simulation meet the mass limit when compared to a 200 h^{-1} Mpc box. The $z = 0.3$ curve comes from the 200 h^{-1} Mpc simulations while the $z = 0.52$ curve comes from the 255 h^{-1} Mpc simulation.

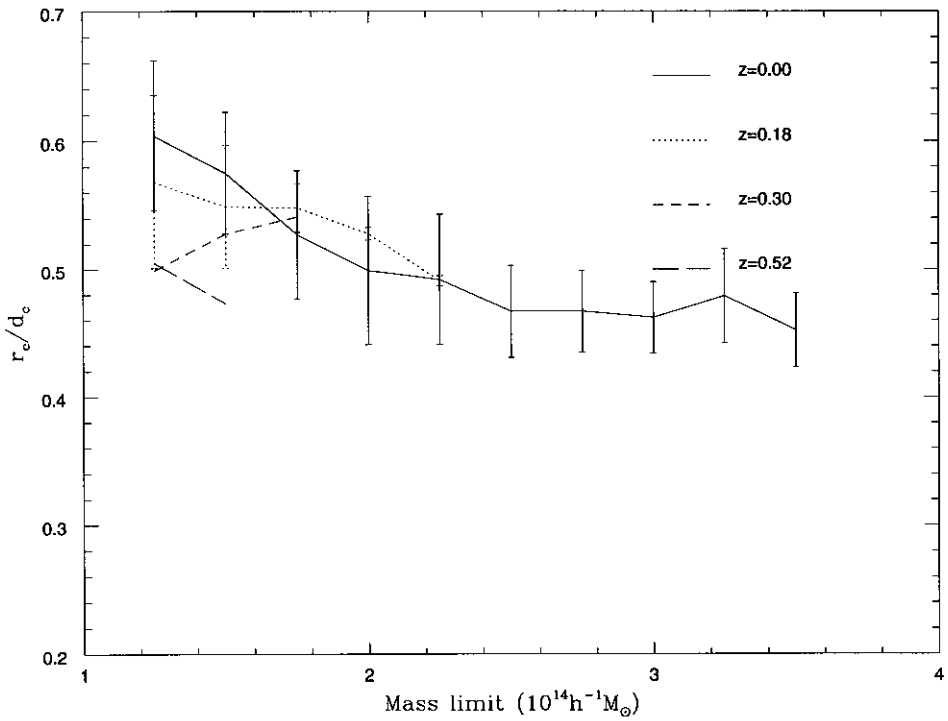

FIG. 6.—Correlation length normalized to the mean separation between clusters. Since the correlation function, and therefore correlation length, is a function of number density, an attempt is made at normalization by dividing the correlation length by the mean separation between clusters. While each sample shows some dispersion, an average of similar redshifts shows an expected leveling off. Errors are determined as in Fig. 5.

where V is the total volume and the parameter σ is related to Q by $\langle Q^2 \rangle = 3\sigma^2$. The rms value of the quadrupole $\langle Q^2 \rangle^{1/2}$ is 0.17, 0.20, and 0.20 for the redshift moments 0, 0.16, and 0.52, respectively. The difference is not statistically significant.

5. EVOLUTION OF VIRIAL PROPERTIES AND DENSITY PROFILES

Using the virial theorem as an estimator yields a mass $M = \alpha R v^2/G$, where v is the velocity dispersion, α is a numerical coefficient, and R is the cluster radius, defined as the Abell radius $R_A = 1.5\ h^{-1}$ Mpc. As a result, all details of the cluster structure are hidden in the coefficient α. Here are some examples: For a spherical cluster with constant density, this parameter is $\alpha = \frac{3}{5}$. For the King model $\rho = \rho_0/[1 + (r/r_c)^2]^{3/2}$ with truncated density at some radius r_{max}, the value of α ranges from 0.6 for $r_{max} \ll r_c$, to 1.21 at $r_{max} = 10r_c$, to 2.67 at $r_{max} = 50r_c$. The general tendency is clear: larger values of α correspond to more centrally condensed clusters. Figure 9 shows the one-dimensional velocity dispersion of dark matter particles against cluster mass for all clusters with $v > 300$ km s^{-1} in the 255 h^{-1} Mpc box. No mass limit is used, so any significant overdensity of cold particles is shown.

In each panel of Figure 9 the majority of the clusters fall along a line $M \propto v^2$ near the top of the panel. For $z = 0$ this line gives a value of α equal to 1.1, which corresponds to $r_{max} = 8r_c$ if we assume a King model, which is in reasonable agreement with our 0.33 h^{-1} Mpc resolution. The existence of the concentration of clusters along the line is quite remarkable. It indicates that the gravitational radius $R_g \equiv \alpha R$ is almost the same for clusters with masses 10^{14}–10^{15} $h^{-1}\ M_\odot$. All clusters below this line have larger velocity dispersions. This might indicate (1) that their radii are smaller than those of "virialized" clusters on the line, (2) that their profiles are steeper (resulting in larger values of α), or (3) a significant degree of merging activity. At first sight, the latter option would seem to be the explanation, but inspection of a few cases with high velocity and low mass shows that it might not be true. The most massive clusters (mass larger than $5 \times 10^{14}\ h^{-1}\ M_\odot$) are the most likely to show evidence of previous mergers. They do not deviate from the $M \propto v^2$ line, but this does not mean that they do not show significant merging or substructure. For example, the largest cluster in Figure 1 consists of two clusters in the process of merging, but altogether it does not show significant deviation from the $M \propto v^2$ line. In addition, we found that clusters with large v are often those that are close to very large nearby clusters or are located between massive clusters. It seems that the tidal field might significantly distort them.

It is interesting to note that while there are many clusters with mass well below that which should be expected for virialized clusters with a given velocity, there are no clusters with mass *above* the virial relation. Observationally, this relation can lead to a significant overestimation of some cluster masses if velocity dispersion is used as the sole constraint. An additional test, such as the examination of a density profile, can provide further insight into the cluster's state of virial equilibrium. This problem is especially remarkable if we try to apply the usual top-hat model for cluster formation. It nicely explains why most massive clusters are on the $M \propto v^2$ line: their overdensity within an Abell radius is above the 170 that is predicted by the model. But clusters with mass $10^{14}\ h^{-1}\ M_\odot$ have an overdensity of only 25. If the model were correct, these are clusters that only recently passed through their turnaround radius and thus should have a velocity *smaller* than their virial velocity. This would place them above the $M \propto v^2$ line. In our simulations we found none of these cases. It seems that the

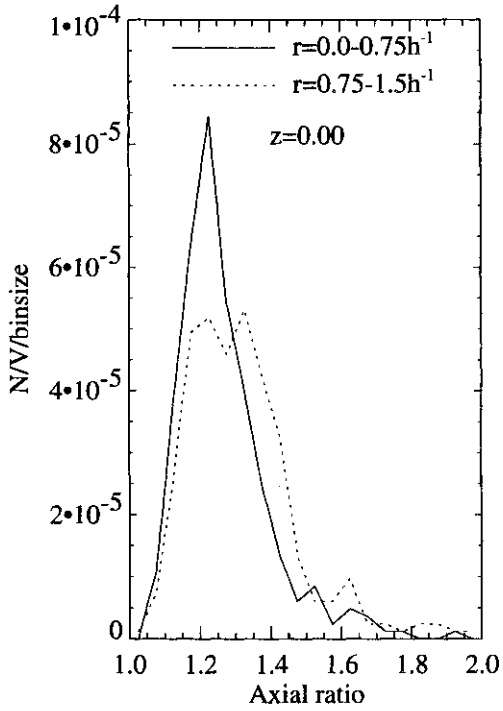

FIG. 7a

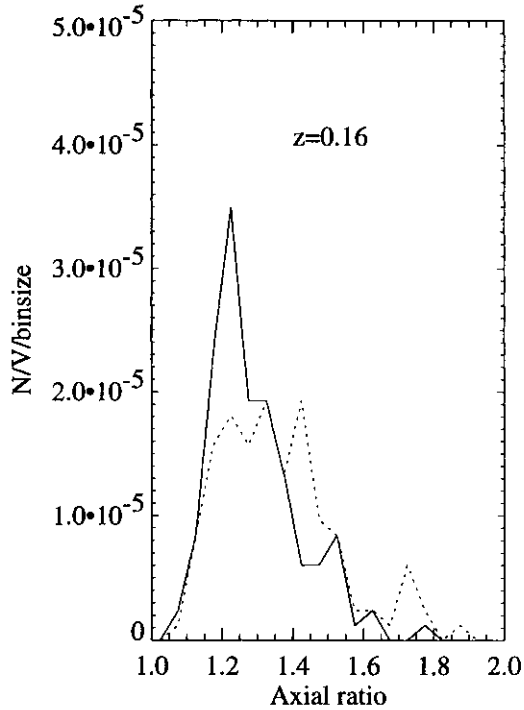

FIG. 7b

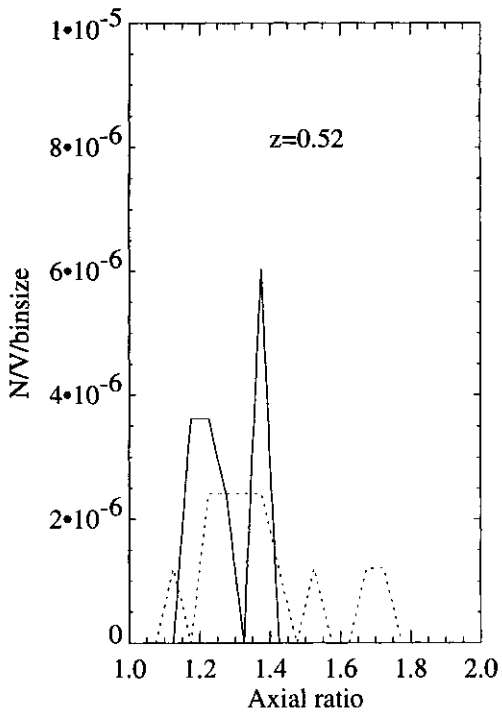

FIG. 7c

FIG. 7.—Histograms of the axial ratio between the largest and smallest radii of the cluster. This is determined by transforming the moment-of-inertia tensor to obtain the principal axes and solving $I = mr^2$ for r. The solid curve shows the inner volume of the cluster while the dashed curve shows the outer annulus. The different epochs are $z = 0.00$ (*left*), $z = 0.16$, (*middle*) $z = 0.52$ (*right*). Each epoch shows the same pattern of greater anisotropy farther from the cluster center. The abscissa is normalized by the volume of the box and the bin size. One cluster is equivalent to $1 \times 10^{-6} h^{-1}$ Mpc^{-3}.

model works reasonably well for massive clusters, which dominate their local environment, but fails for small clusters, which are dominated by this environment.

In all three epochs the solid line in Figure 9 is the fit for the $z = 0$ case. With increasing redshift the fit for each epoch (*dashed lines*) moves down, which shows that a cluster with the same mass had higher velocity dispersion in the past. This is due to a change in the overall shape of the cluster from being core-dominated at $z = 0.52$ to having a larger contribution from outer regions in the present epoch. With more of the cluster mass near the core in the past, it would be easier to have an increased velocity. In order to check this, we studied the density profile in the most massive clusters. Those with one-dimensional velocity dis-

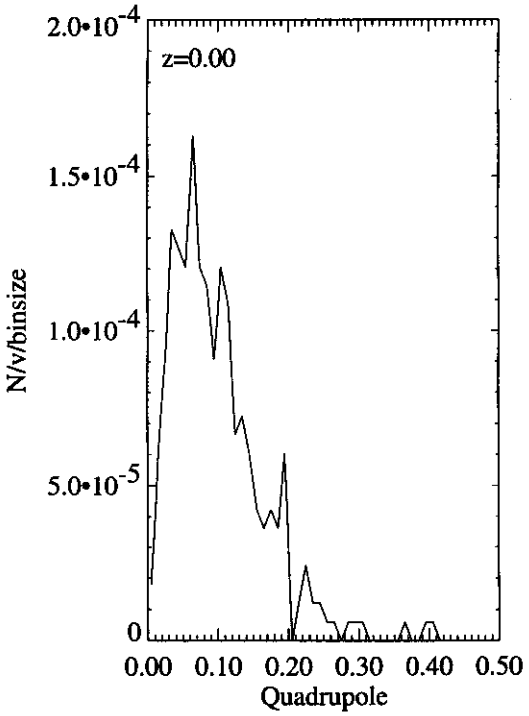

FIG. 8*a*

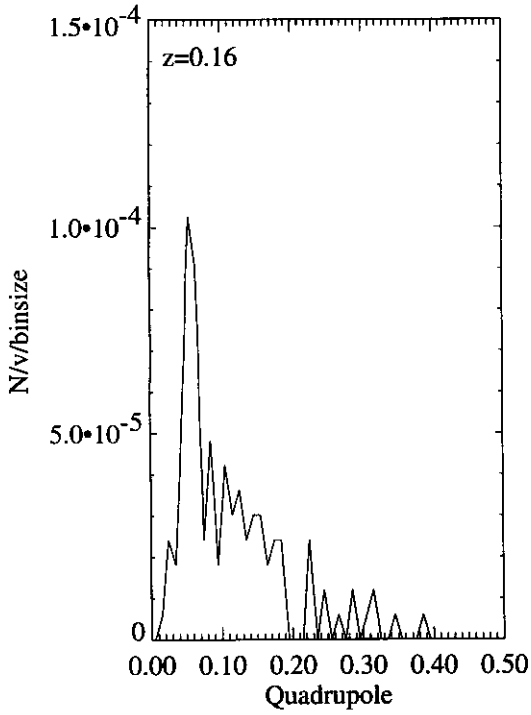

FIG. 8*b*

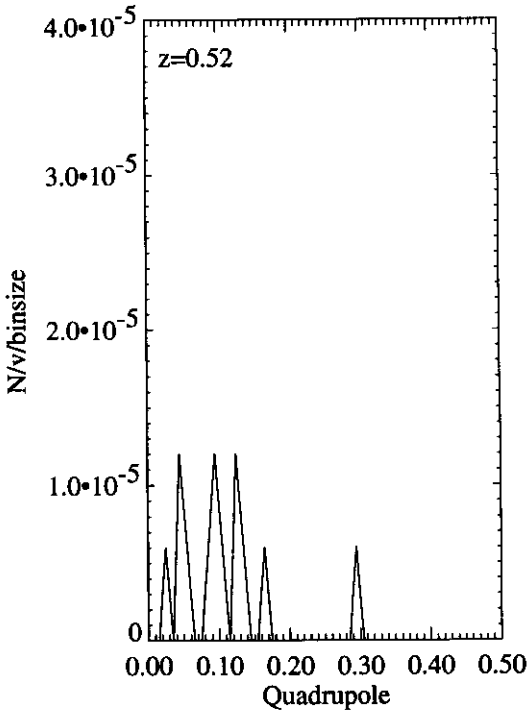

FIG. 8*c*

FIG. 8.—Distribution of the quadrupole of the cluster anisotropy. Epochs and normalization are as in Fig. 7. The anisotropy does not appear to vary with redshift.

persions between 855 and 1000 km s^{-1} are considered for their density profiles as shown in Figure 10. The average density profile has been computed at the two extreme redshifts. For the $z = 0$ case, 19 clusters were used, and four clusters for $z = 0.52$. Near the center the profiles are unresolved and look similar, but the drop-off in density happens at relatively large radii and is numerically resolved. It appears to be much steeper for the clusters at large redshifts. Two dashed lines with power laws approaching that of the outer regions are drawn alongside for comparison. The dash-dot-dashed lines show fits to the profiles. We used the King approximation for the fits: $\rho/\langle\rho\rangle \propto [1 + (r/r_c)^2]^{-\alpha/2}$. For $z = 0$ this fit yields $\alpha \approx 3$, and for $z = 0.52$ the slope is $\alpha \approx 5$.

In order to check that these results are not affected by the finite resolution of our numerical simulations, we traced the evolution of the two most massive clusters in our 5 times higher resolution simulation (box size 50 h^{-1} Mpc,

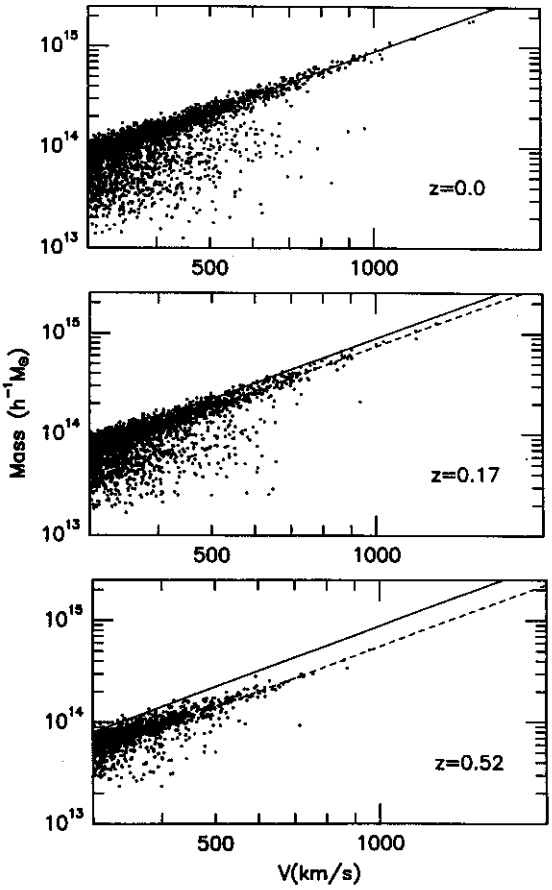

FIG. 9.—Mass vs. velocity at three separate epochs. The solid line is th fit to the $z = 0.0$ case, while dashed lines are fits to the individual epochs. All clusters with velocity dispersions above 300 km s^{-1} are shown.

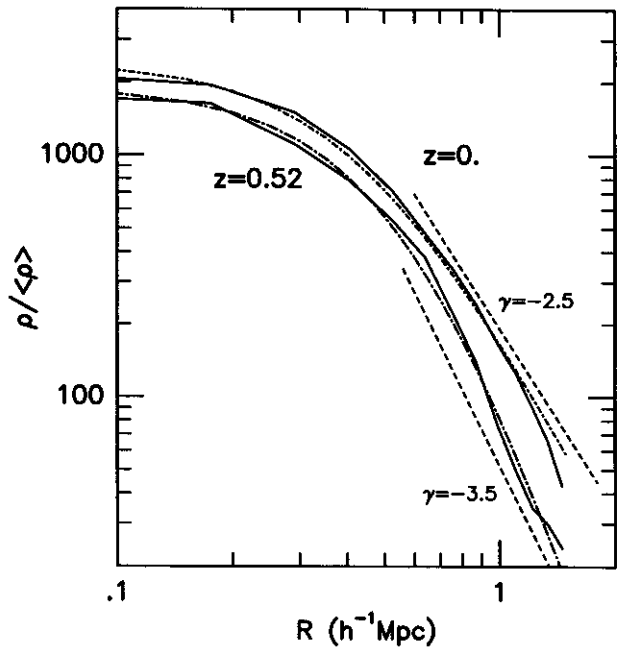

FIG. 10.—Average density profile for clusters with velocity dispersions between 855 and 1000 km s^{-1}. The top solid curve is for $z = 0$ and the bottom solid curve is for $z = 0.52$. The dash-dot-dashed curves are fits to the two profiles. Functions are given in the text. Dashed lines are power laws of the given γ.

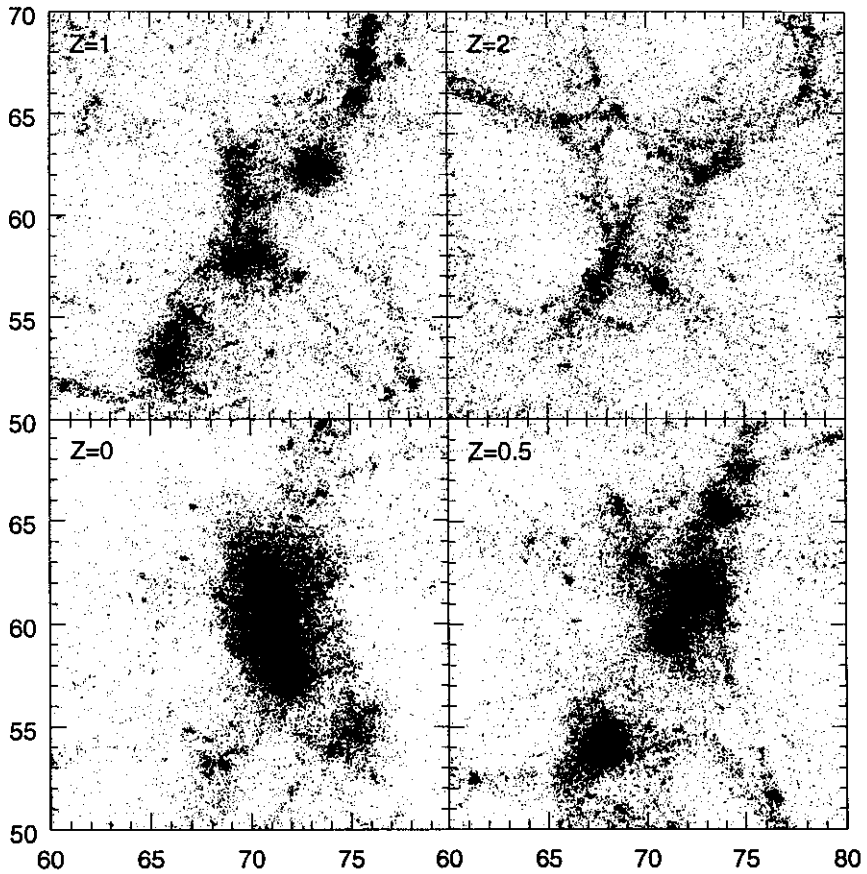

FIG. 11.—Distribution of CDM inside a 10 h^{-1} Mpc box around one of the clusters at different redshifts. The cluster is slightly above the center of the box at $z = 0$. There is another (smaller) cluster few a megaparsecs away. The fraction of particles shown for $z = 0$ is 2 times smaller than for the other moments.

resolution 62.5 h^{-1} kpc). Figure 11 shows the distribution of CDM inside a 10 h^{-1} Mpc box around one of the clusters at different redshifts. The cluster is slightly above the center of the box at $z = 0$. There is another (smaller) cluster a few megaparsecs away. The fraction of particles shown for $z = 0$ is 2 times smaller than for the other moments. At $z = 1$ the cluster is much smaller and its center is at $x = 73$ Mpc, $y = 62$ Mpc (note that the axes are not scaled with h). At $z = 2$ the cluster is at the same position, but it is merely a very large halo with mass $\sim 10^{12}$ $M_\odot$. It is interesting to note how drastically the distribution of matter changes with time. At $z = 0$ most of the halos (tiny knots of particles seen in the figure) are found very close to the clusters, with some indication of a filament oriented vertically on the plot. At $z = 0.5$ the distribution is dominated by group-sized objects. The filament is more prominent and there are some halos away from the center. At $z = 1$ the filament is the most prominent structure. Groups are smaller, but still visible, and many halos are outside the filament. At $z = 2$ the filament has not yet formed. There are many small-sized filaments and relatively large halos.

Figure 12 shows the density profile of two large clusters [$M = (4\text{–}5) \times 10^{14}$ h^{-1} $M_\odot$] at $z = 0$ and $z = 1$. The bottom panels present the overdensity of CDM particles, with a distance scale given in comoving coordinates. Dashed curves are analytical fits of the form $\delta_0/[1 + (r/r_c)^2]^{\alpha/2}$. For both clusters we used the same core radii and slopes. At $z = 0$ we found $r_c = 0.070$ h^{-1} Mpc and $\alpha = 2.30$. For $z = 1$, the fits gave $r_c = 0.085$ h^{-1} Mpc and $\alpha = 2.70$. The core radii are still not resolved. The slope of the density profile indicates the same trend as in our low-resolution simulations (though with smaller differences): steeper profiles in the past. In order to directly compare profiles at different redshifts we plot the absolute density in units of mass of hydrogen atom per unit volume in the top panels. A shift is noticeable for the $z = 1$ component because the radius is plotted in proper coordinates (the virial theorem requires a proper, not a comoving, radius). Now the difference in slopes is more clear. Because our resolution is unchanging in comoving coordinates, the very central part of the cluster is better resolved in the past: in proper coordinates the resolution at $z = 1$ is twice that at $z = 0$. This explains why the density is higher at the center at $z = 1$. In any case, the mass within the central 100 kpc

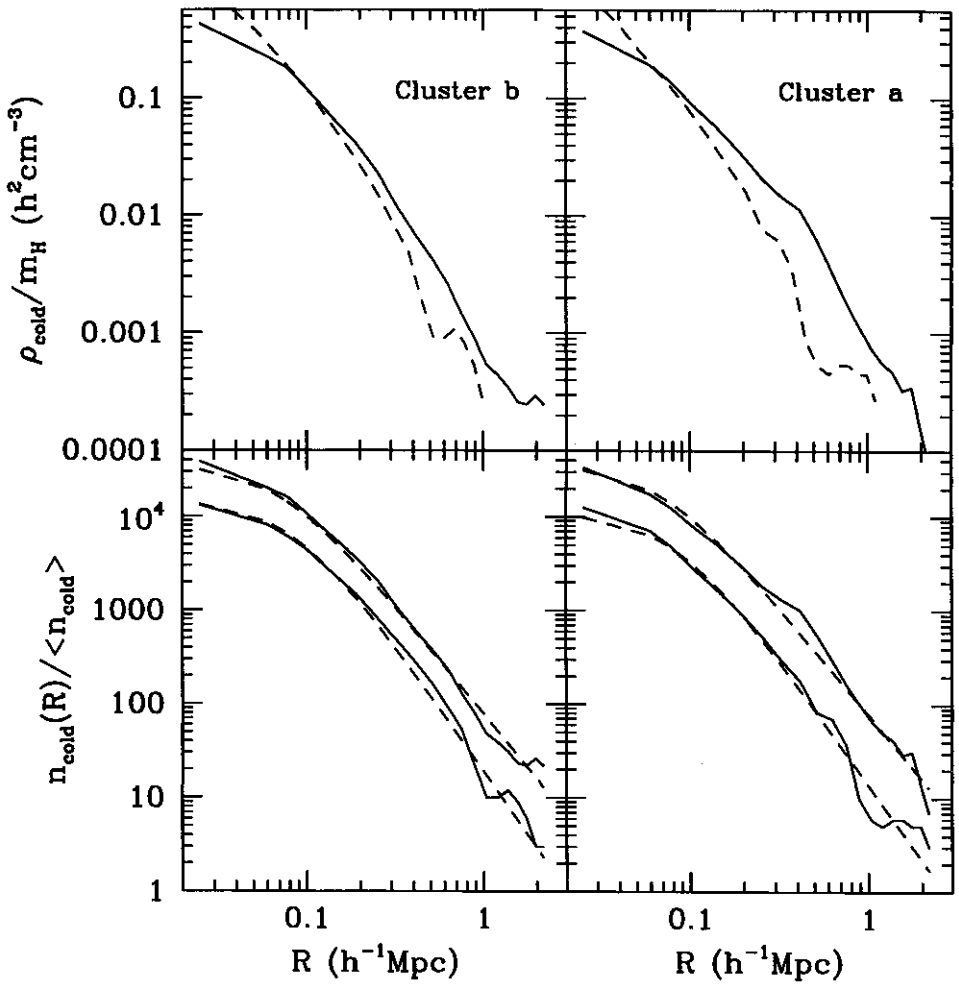

FIG. 12.—Density profile of two large clusters [$M = (4\text{–}5) \times 10^{14}$ h^{-1} $M_\odot$] at $z = 0$ and $z = 1$. Bottom panels present the overdensity of CDM particles (*solid curves*) with a distance scale given in *comoving coordinates*. Dashed curves are analytical fits $\delta_0/[1 + (r/r_c)^2]^{\alpha/2}$, with $r_c = 0.070$ h^{-1} Mpc and $\alpha = 2.30$ for $z = 0$. For $z = 1$, the fits gave $r_c = 0.085$ h^{-1} Mpc and $\alpha = 2.70$. In the top panels the solid line represents $z = 0$ and the dashed line $z = 1$. They show the absolute density in units of mass of hydrogen atom per unit volume. *Radius is plotted in proper coordinates.* Because the earlier epoch is further resolved, it appears to have a sharper central peak; however, there is no change with redshift over the inner 100 h^{-1} kpc.

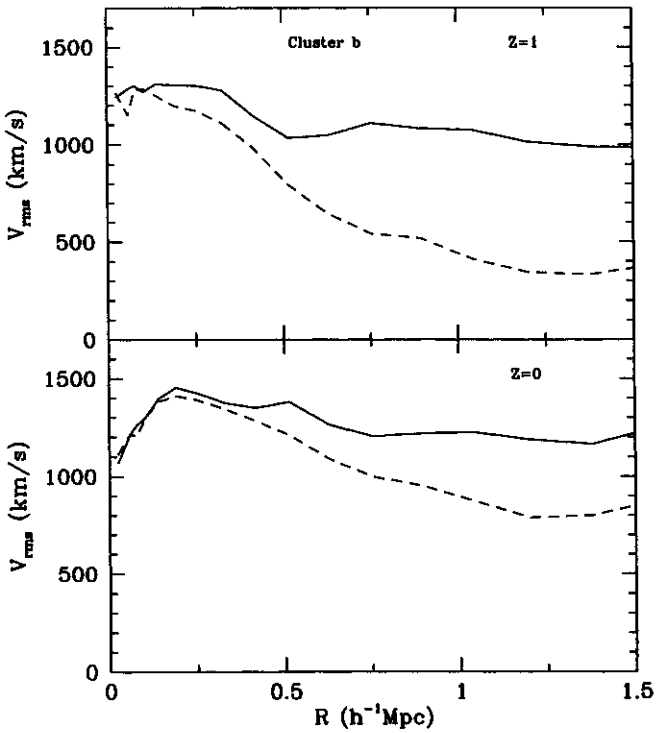

FIG. 13.—Three-dimensional rms velocity profiles for a cluster at $z = 0$ and $z = 1$. Solid curves are for the total velocity. Some part of this velocity is due to streaming of material inside the cluster. The dashed curves show the chaotic rms velocity on a 150 h^{-1} kpc scale. At $z = 1$, velocities outside the central 0.5 Mpc region are mainly in the streaming component. At $z = 0$ the chaotic velocities are much larger and dominate.

radius does not change over time. What does change is the density in the peripheral parts of the clusters—it increases by an order of magnitude.

While the density in peripheral parts (and thus the total mass) evolves quite significantly with time, the velocity dispersion is much more stable. Figure 13 shows three-dimensional velocity profiles for a cluster at $z = 0$ and $z = 1$ (*solid curves*). Some part of this velocity is due to streaming of material inside the clusters. It is interesting to estimate how large that streaming velocity is when compared with the truly chaotic component. We estimated the chaotic velocity in the following way: We found the velocity of each CDM particle relative to the velocity of cold matter inside a sphere of 150 h^{-1} kpc radius centered on the particle. If there were no streaming velocities, the sphere would not move and the rms relative velocity would be just the same as the rms velocity of all dark matter in the cluster. In the other extreme case, when there are large clumps moving inside clusters with relatively small velocities of internal motion inside the clumps, we would expect the relative (chaotic) velocity to be significantly smaller than the total rms velocity. In reality, the situation is always somewhere in between. The central 0.5 Mpc part seems to be quite relaxed (the two velocities being close) while the peripheral parts show some degree of ongoing evolution. The dashed curves in Figure 13 show the chaotic rms velocity on a 150 h^{-1} kpc scale. At $z = 1$, velocities outside the central 0.5 Mpc region are mainly in the streaming component. At $z = 0$ the chaotic velocities are much larger and dominate.

6. CONCLUSIONS

We have studied properties of clusters at different redshifts as predicted in the CHDM model. Effects of the correlation function, anisotropies, and density profiles were examined. We find that the correlation function for clusters of the same mass limit was larger and steeper at high redshifts. The slope increases from 1.8 at $z = 0$ to 2.1 at $z = 0.5$. The comoving correlation length r_c scales with the mass limit M within comoving radius 1.5 h^{-1} Mpc and the redshift z as $r_c \approx 20(1 + z)(M/M_*)^{1/3}$, where $M_* = 3 \times 10^{14}$ h^{-1} $M_\odot$. When the correlation length is normalized to the mean cluster separation d_c, it remains almost constant: $r_c \approx (0.45\text{–}0.5)d_c$. For small masses of clusters ($M < 2 \times 10^{14}$ h^{-1} $M_\odot$) there is an indication that r_c goes slightly above the relation, with the constant of proportionality being $\sim$0.55–0.6.

Examining isotropies, we place rough limits on what is a normal or nearly relaxed cluster. We show that average shapes of clusters do not change significantly over time even in the outer 1–2 Mpc parts of clusters, where the resolution of our simulations is adequate for the problem. There is some evidence showing that the small number of highly anisotropic clusters virialize over time, but more statistics are needed here. We also found that the cores of clusters (inner 0.5 Mpc) remain nearly the same for redshifts $z = 0$–1 while the outer regions show definite continual accretion and change of slope of the density profile.

Finally, we can see some evidence for evolution by studying the virial properties of the clusters. The outlying regions of the clusters grow denser and have lower velocity dispersions at the present epoch for the same mass. Our evidence shows that the majority of clusters have apparently been effectively virialized. The gravitational mass of those that have not is universally smaller than expected for their mass. Thus, for these clusters it is not accurate to assign masses simply by using the virial theorem and the velocity dispersion. Power-law fits for density profiles in $\Omega = 1$ universes at $z = 0$ have been shown to range between 2.2 and 2.5, consistent with our results (Crone, Evrard, & Richstone 1994). Our evidence points to clusters' continuing to accrete matter over time but retaining their basic symmetry.

REFERENCES

Abell, G. O. 1958, ApJS, 3, 211
Bahcall, N. A., & Burgett, W. S. 1986, ApJ, 300, L35
Bahcall, N. A., & Cen, R. 1992, ApJ, 398, L81
———. 1993, ApJ, 407, L49
Bahcall, N. A., & Soneira, R. M. 1983, ApJ, 270, 20
Bahcall, N. A., & West, M. J. 1992, ApJ, 392, 419
Bartlett, J. G., & Silk, J. 1993, ApJ, 407, L45
Biviano, A., Girardi, M., Giuricin, G., Mardirossian, F., & Mezzetti, M. 1993, ApJ, 411, L13
Borgani, S., Coles, P., & Moscardini, L. 1994, MNRAS, 271, 223
Borgani, S., Plionis, M., Coles, P., & Moscardini, L. 1995, MNRAS, 277, 1191
Bryan, G. L., Klypin, A., Loken, C., Norman, M. L., & Burns, J. O. 1994, ApJ, 437, L5
Castander, F. J., Ellis, R. S., Frenk, C. S., Dressler, A., & Gunn, J. E. 1994, ApJ, 424, L79
Cen, R., & Ostriker, J. P. 1994, ApJ, 431, 451
Croft, R. A. C., & Efstathiou, G. 1994, MNRAS, 267, 390
Crone, M. M., Evrard, A. E., & Richstone, D. O. 1994, ApJ, 434, 402
Dalton, G. B., Croft, R. A. C., Efstathiou, G., Sutherland, W. J., Maddox, S. J., & Davis, M. 1994, MNRAS, 271, L47
Dalton, G. B., Efstathiou, G., Maddox, S. J., & Sutherland, W. J. 1992, ApJ, 390, L1
Gunn, J. E. 1990, in Clusters of Galaxies, ed. W. Oergerle, M. J. Fitchett, & L. Danly (Cambridge: Cambridge Univ. Press), 341
Holtzman, J., & Primack, J. 1993, ApJ, 405, 428
Hughes, J. P. 1989, ApJ, 337, 21
Jing, Y.-P., & Fang, L.-Z. 1994, ApJ, 432, 438

Jing, Y.-P., Mo, H.-J., Börner, G., & Fang, L.-Z. 1993, ApJ, 411, 450
Klypin, A., Borgani, S., Holtzman, J., & Primack, J. 1995, ApJ, 444, 1
Klypin, A., Holtzman, J., Primack, J., & Regős, E. 1993, ApJ, 416, 1
Klypin, A., & Kopylov, A. I. 1983, Soviet Astron. Lett., 9, 41
Klypin, A., & Rhee, G. 1994, ApJ, 428, 399 (KR94)
Krauss, L. M., & Kernan, P. J. 1994, ApJ, 432, L79
Luppino, G. A., & Gioia, I. M. 1995, ApJ, 445, L77
Ma, C.-P., & Bertschinger, E. 1994, ApJ, 434, L5
Nichol, R. C., Collins, C. A., Guzzo, L., & Lumsden, S. L. 1992, MNRAS, 255, 21
Peacock, J. A., & West, M. J. 1992, MNRAS, 259, 494
Peebles, P. J. E. 1980, The Large-Scale Structure of the Universe (Princeton: Princeton Univ. Press)
Postman, M., Huchra, J. P., & Geller, M. J. 1992, ApJ, 384, 404
Press, W. H., Teukolsky, S. A., Vettering, W. T., & Flannery, B. P. 1992, Numerical Recipes in C (Cambridge: Cambridge Univ. Press)
Primack, J., Holtzman, J., Klypin, A., & Caldwell, D. O. 1995, Phys. Rev. Lett., 74, 2160
Sutherland, W. J. 1988, MNRAS, 234, 159
Thimm, G. J., & Belloni, P. 1994, A&A, 289, L27
Walker, T. P., Steigman, G., Schramm, D. N., Olive, K. A., & Kang, H.-S. 1991, ApJ, 376, 51
White, D. A., & Fabian, A. C. 1995, MNRAS, 273, 72
White, S. D. M., Efstathiou, G., & Frenk, C. S. 1993a, MNRAS, 262, 1023
White, S. D. M., Navarro, J. F., Evrard, A. E., & Frenk, C. S. 1993b, Nature, 366, 429